arXiv:1603.05172v1 [cond-mat.mes-hall] 16 Mar 2016

Resonance effects in the Raman scattering of mono- and few layers $MoSe_2$

P. Soubelet,[1] A. E. Bruchhausen,[1] A. Fainstein,[1] K. Nogajewski,[2] and C. Faugeras[2,*]

[1] *Instituto Balseiro and Centro Atómico Bariloche, C.N.E.A., R8402AGP Bariloche, Río Negro, Argentina*

[2] *LNCMI (CNRS, UJF, UPS, INSA), BP 166, 38042 Grenoble Cedex 9, France*

(Dated: March 17, 2016)

Using resonant Raman scattering spectroscopy with 25 different laser lines, we describe the Raman scattering spectra of mono- and multi-layers 2H-molybdenum diselenide ($MoSe_2$) as well as the different resonances affecting the most pronounced features. For high-energy phonons, both A- and E- symmetry type phonons present resonances with A and B excitons of $MoSe_2$ together with a marked increase of intensity when exciting at higher energy, close to the C exciton energy. We observe symmetry dependent exciton-phonon coupling affecting mainly the low-energy rigid layer phonon modes. The shear mode for multilayer displays a pronounced resonance with the C exciton while the breathing mode has an intensity that grows with the excitation laser energy, indicating a resonance with electronic excitations at energies higher than that of the C exciton.

PACS numbers: 73.22.Lp, 63.20.Kd, 78.30.Na, 78.67.-n

Layered transition-metal dichalcogenides (MX_2) are today the subject of intense studies because of the possibility to isolate a single monolayer, a two dimensional crystal, out of the bulk material[1,2]. This family of materials includes semiconducting compounds (MX_2 with M=Mo or W and X= S, Se, or Te). They offer an interesting platform to explore purely two-dimensional excitons, phonons, and to study the interplay between the spin and valley physics[3,4]. Monolayers of these materials can be transferred on adapted substrates for optical or transport investigations. In contrast to gapless graphene, their band gap of $1-2$ eV allows for the construction of transistors[5] and of photodetectors[6]. Even though the room temperature electronic mobilities they exhibit reach only the level of few hundreds $cm^2.V^{-1}.s^{-1}$, orders of magnitude below what is achieved in conventional III-V or II-VI semiconductors quantum wells, their flexibility and transparency are extremely appealing for future electronic and optoelectronic applications. For instance, they are used as building blocks of van der Waals heterostructures[7–9], which cannot be controlled without a deep knowledge of the phonon modes and of the electron-phonon interaction in the individual layers. It is also worth to point out that the photoluminescence (PL) of MX_2 monolayers arises from tightly bound excitons[10,11], with binding energies close to 400 meV, and hence comparable to those usually observed in molecules or in carbon nanotubes[12,13].

Raman scattering plays an important role in the rapid development of the field of research of 2D crystals as it provides, for most layered materials, a fast and non-invasive tool to determine the number of layers of a given specimen[14]: When the thickness of a MX_2 flake is reduced, the energy of some optical phonons changes in a way that can be traced using standard techniques. Resonant Raman scattering is powerful technique to explore electronic properties of materials. The resonant enhancement of Raman scattering signals when the laser energy is tuned to particular values corresponding to electronic excitations of the investigated system, is a well established tool to perform, for instance, the spectroscopy of weakly radiative excitations. This technique has been applied to MoS_2 thin layers, probably the most explored layered MX_2 so far, and to WSe_2[15–19].

The Raman spectrum of bulk 2H-$MoSe_2$ has been measured in 1980[20], allowing for the identification of the main Raman-active phonon modes of this compound. Since that time, only few studies reported the Raman spectrum of thin layers of this material[21–23]. Although they provided the description of the main phonon modes, a complete characterization of the Raman scattering spectrum of thin layers of $MoSe_2$ is still lacking. The phonon band structure of monolayer $MoSe_2$ has recently been calculated by ab-initio techniques[24], and this compound appears to be distinct from other member of the MX_2 family. All these materials present 6 optical and 3 acoustical phonon branches, but, in contrast to the case of MoS_2, WS_2 or WSe_2[25], according to these calculations, in $MoSe_2$ the A'$_1$ mode is located between the E' and E" modes and is not the highest Raman-active mode at the Γ point of the phonon band structure. The phonon mode of E symmetry around 290 cm^{-1}, measured at 632.8 nm, has a much weaker intensity than the A_1 mode[23] close to 243 cm^{-1}. The E' mode is split over the whole phonon Brillouin zone, with a splitting of ~ 4 cm^{-1} at the Γ point. These two E' phonons are of longitudinal (LO) and of transverse character (TO), and their splitting comes from the polar character of $MoSe_2$.

Resonant studies with a large number of laser lines spanning from the near infrared to the ultraviolet are seldom done, and this is particularly difficult and absent in the literature when low energy excitations are involved. It is such a systematic and comprehensive study that is being reported here, for a model MX_2 material ($MoSe_2$) from monolayer to multi-layer structures. We present a resonant Raman scattering investigation of mono- and multilayer 2H-$MoSe_2$ using 25 different laser excitation lines from 458 nm (2.7 eV) to 825 nm (1.5 eV), which

span the energies of the three different excitons A, B and C, located close to 1.54, 1.74 and 2.61 eV, respectively[26], and including both high and low energy vibrations. In the first part, we focus on monolayer $MoSe_2$ (1L-$MoSe_2$), discussing in particular the identification of the main Raman scattering features and their excitation profiles. We then address the case of multilayer $MoSe_2$ (NL-$MoSe_2$ where N is the number of layers) and describe the phonon modes which are only Raman-active in multilayers. These modes have been observed in $MoTe_2$[27–29], MoS_2[18], WSe_2[30,31], and we propose here their proper identification in $MoSe_2$, based on polarization resolved measurement and on resonant Raman scattering experiments. We present the excitation profiles of the main Raman features, including the low energy shear and breathing modes in the case of 2L-$MoSe_2$, and provide evidence, for some of these modes, of an increase of the scattering efficiency at energies beyond that of the C exciton.

Raman scattering experiments were performed at room temperature in the backscattering geometry with a triple-grating spectrometer equipped with a nitrogen cooled charge coupled device (CCD) camera. Laser excitation was provided by a mixed Ar/Kr laser (from 458 to 676 nm) and by a Ti:Sapph laser (from 680 nm to 825 nm). Laser lines were filtered with a grating used in the Littrow configuration. A 50x objective was used to focus the excitation laser down to a spot of 2 μm, with optical power of 0.4 mW. Thin flakes of $MoSe_2$ were first exfoliated from bulk $MoSe_2$ purchased from *HQ graphene* and then deposited on a Si/SiO_2 substrate with a SiO_2 thickness of 90 nm. Flakes composed of 1 to 8 layers were identified by their different optical contrast contrast (calibrated with AFM measurements on other flakes) and then by low energy Raman scattering and photoluminescence experiments. Raman scattering spectra were normalized by the integrated intensity of the silicon peak and by its resonant excitation wavelength dependence[32], and by the effect of interferences in the SiO_2 layer[33] (see appendix). The luminescence background in the case of 1L and 2L has been removed from the presented spectra. In the following, the intensity of each mode is normalized to its maximum value observed in the investigated excitation energy range. We are interested in the independent evolution of the different modes and not by their relative intensities. The vibration patterns of MX_2 has been described in many recent reports[34,35]. Bulk 2H-MX_2 belongs to the D_{6h} point group, while their odd and even few layers counterparts represent the D_{3h} and D_{3d} point groups, respectively. This implies a change of the symmetry of the phonon modes depending on the number of layers. In what follows we will use the previously introduced notation[18], indicating the symmetry of the different phonon modes by a double notation corresponding to the odd and even number of layers.

In Fig. 1a-c we present three Raman scattering spectra of monolayer $MoSe_2$ measured at 465 nm (panel a), at 676 nm (panel b) and at 735 nm (panel c). The scale of these spectra is set in order to compare the position of the different features and normalized spectra are presented in Fig. 1d. With a 465 nm excitation, the most prominent feature is the A'$_1$ mode observed at 242 cm^{-1} in 1L-$MoSe_2$. Its intensity is 10 times bigger than the intensity of all other Raman scattering features. The E' mode, predicted to be Raman-active in Ref. [24] is also observed at 288 cm^{-1}. These are the two main features of the Raman scattering spectrum of 1L-$MoSe_2$[21–23,36].

A more detailed investigation shows that, similar to other MX_2[15,37–40] compounds, acoustical phonons also contribute to the Raman scattering spectrum of 1L-$MoSe_2$ and that depending on the excitation wavelength, such contribution can be strongly enhanced (see e.g. the spectra measured using 676 nm and 735 nm laser excitations). Because the dispersion of acoustical phonons close to the M and K points is rather flat[24], the associated density of states is peaked close to this energy and defect mediated phonon scattering is favored. We observe the longitudinal acoustical phonon from the M-K points (LA(M)) at 152 cm^{-1} and its first overtones (2LA(M), 3LA(M) and 4LA(M)). Next we see a combination of optical and acoustical phonons from the M point, namely A'$_1$(M)$\pm$LA(M) at 61 and 364 cm^{-1}, respectively, A'$_1$(M)+2LA(M) at 518 cm^{-1}, and E'(M)+LA(M) as well as E'(M)+2LA(M) at 432 and 584 cm^{-1}, respectively. One can also notice in our experimental data the TA(M)+ XLA(M) with X= 1 to 3 at 262, 414 and 568 cm^{-1}. These acoustical phonons features are observed on freshly exfoliated $MoSe_2$ flakes, and also, with similar intensity, on flakes produced 6 months before.

An additional Raman scattering feature appears at 252 cm^{-1} on all samples, mono- or multilayers. Polarization-resolved measurements show that this feature is of the A-type symmetry, and it follows the same resonances, discussed in the following, as the main A'$_1$ feature at 242 cm^{-1}. At high excitation energy, we also observe some traces of the modes E" (Γ) and A"(Γ) at 170 and 354 cm^{-1}, respectively[24,25], which are normally forbidden for mono-layers in back scattering geometry.

When decreasing the excitation energy using 676 nm or 735 nm excitation (Fig. 1b,c), the Raman scattering spectrum of 1L-$MoSe_2$ changes drastically: the A'$_1$ feature at 242 cm^{-1}, which is prominent at higher excitation energy now has an intensity comparable to that of the acoustical phonon features and of their overtones. The mode TA(M)+LA(M), at 262 cm^{-1} and the LA(M) overtones also become particularly well visible in this excitation energy regime. The E'(Γ) phonon, previously observed at 289 cm^{-1} now appears at slightly higher energy 292 cm^{-1}, which we tentatively interpret, based on the phonon band structure calculations[24], as the selective excitation, for different excitation laser energies, of the lower-energy TO mode or of the upper-energy LO mode[24]. This crossover is presented in more details in Fig. 2. The lower component of the split E' mode, prominent for excitation wavelengths below $\sim$ 500 nm, gradually disappears as the excitation wavelength increases.

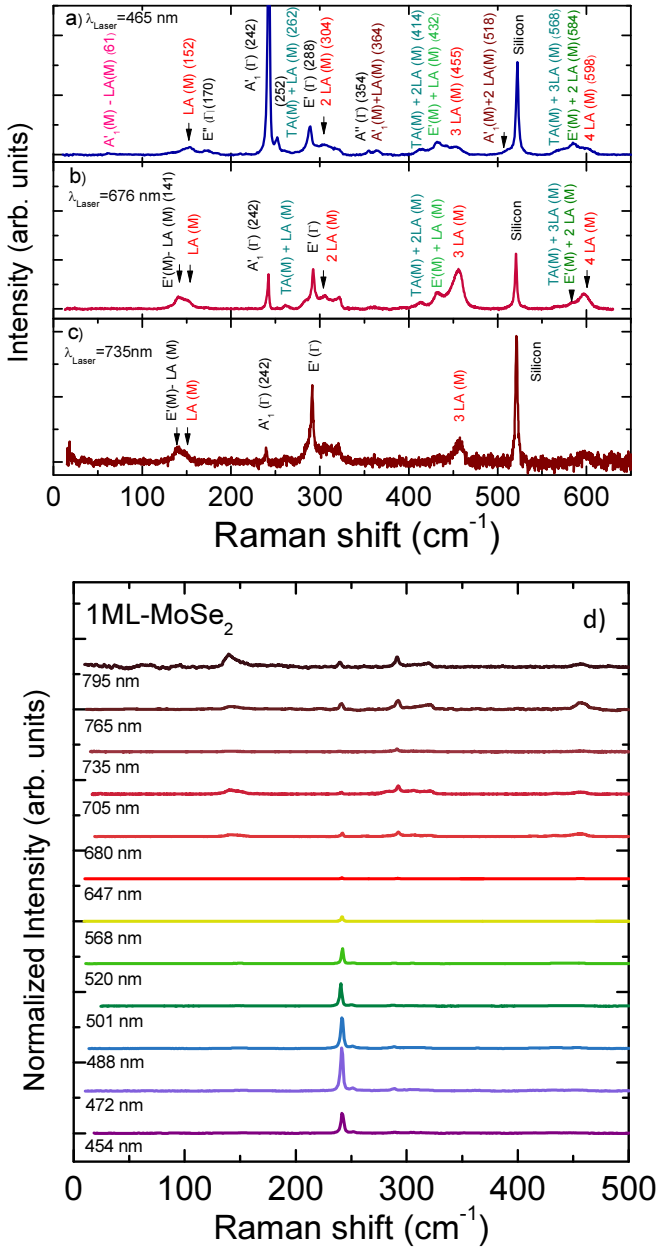

Figure 1. Raman scattering spectra of monolayer $MoSe_2$ measured with a) 465 nm, b) 676 nm and c) 735 nm laser excitation. The main Raman scattering features are identified in the figure and the intensity scale is set in order to see the features for all excitations wavelengths. d) Normalized Raman scattering spectra for the monolayer.

Above $\sim$ 600 nm, the upper component of the split E' phonon appears at 292 cm^{-1} with an intensity increasing with the excitation wavelength. As will be confirmed in the following, this behavior suggests a preferential coupling of the LO phonon with the A- and B-type excitons, while the TO phonon can only be observed when exciting at high-energy, in the C exciton range of energy. Such an effect, pronounced in 1L-$MoSe_2$, is also observed in multilayers even though they do not exhibit too strong

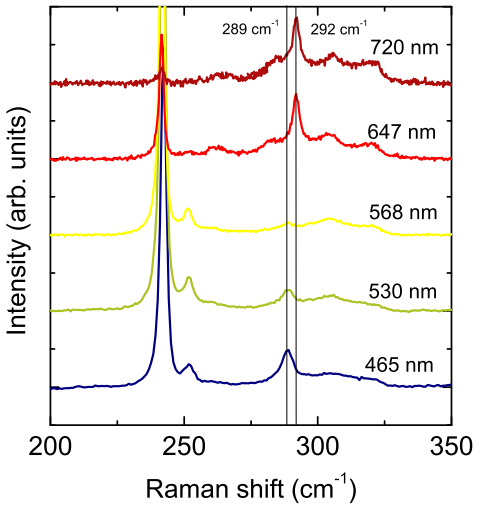

Figure 2. Raman scattering spectra of monolayer $MoSe_2$ measured with 465 nm, 530 nm, 568 nm, 647 nm and 720 nm laser excitation showing the selective excitation of the two E' optical phonons.

E'/E_g feature for low excitation energies. We do not have a microscopic explanation for this crossover and for the resonant behavior. Electronic band structure calculations, together with a phonon mode analysis might help in understanding this effect. Such analysis are beyond the scope this experimental paper.

The Raman scattering spectrum of multilayers of $MoSe_2$ shows some additional features. As can be seen in Fig. 3a for 1L- to 5L-$MoSe_2$ two additional peaks, marked by the red boxes, appear at 170 and 354 cm^{-1} respectively. The energy of these two modes does not depend on the number of layers. In Fig. 3b, we present two Raman scattering spectra measured on a 2L-$MoSe_2$ in the co- and cross-linear polarization configurations. In the cross-linear configuration, the A_{1g} mode at 242 cm^{-1} is suppressed, together with the mode observed at 354 cm^{-1}, showing that this mode is of A-type symmetry. The feature observed at 170 cm^{-1} is not affected by the polarization configuration and exhibits hence E-type symmetry. These two features observed at 170 cm^{-1} and at 354 cm^{-1} are then attributed to the zone center E"/E_{1g} and A"$_2$/A_{1g}, respectively, and they are not Raman-active in monolayers (even though they show up as weak features when using high excitation energies). Similar Raman scattering results have been recently obtained on MoS_2[18] and the A"$_2$/A_{1g} was observed in WSe_2[31]. These latter two modes are not observed in the $MoSe_2$ monolayer, and, as in the case of MoS_2, they only appear in multilayers for excitation energies close to the C-exciton energy. The effect have been clearly observed in MoS_2[18] and these authors explained this observation by the fact that, in contrast to the low-energy A and B

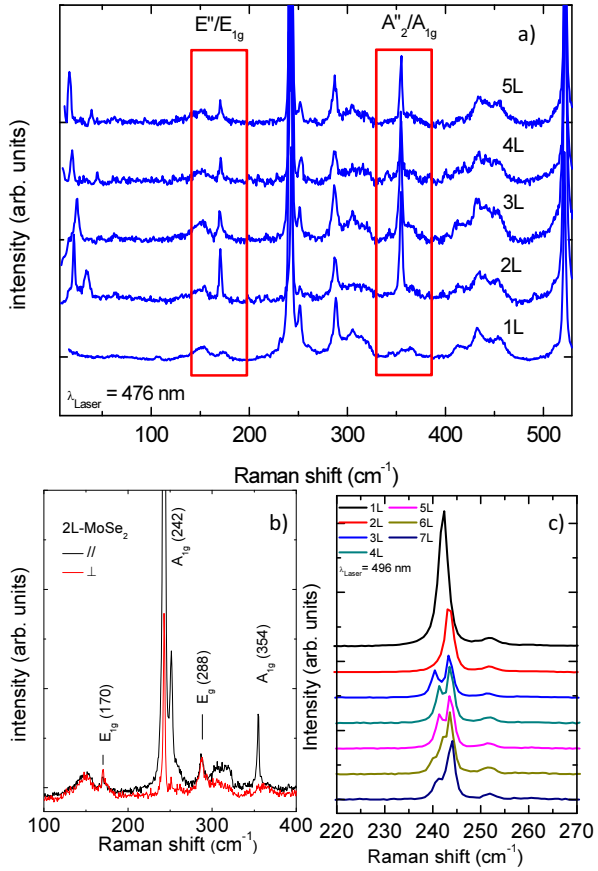

Figure 3. a) Raman scattering spectra of 1 to 5 layer $MoSe_2$ recorded with the use of 465 nm excitation showing the E" and A"$_2$ phonons at 170 and 354 cm^{-1}, respectively. b) Polarization resolved Raman scattering spectra of 2L-$MoSe_2$ measured with 514 nm and identifying the two E and A type phonons. c) A'$_1$/A$_{1g}$ feature for 1- to 7- layers $MoSe_2$ samples.

excitons whose wave-functions are strongly confined to individual layers, the C exciton's wave-function is delocalized along the whole structure[41,42]. As a results, the C exciton can effectively couple to those phonon modes which are characteristic of multilayers and a resonance of the scattered intensity is observed for laser energies close to the C-exciton energy. On the other hand, features of this type do not appear at lower excitation energies, corresponding to the A and B excitons[18]. The observation of these two Raman features can help to quickly discriminate between mono- and multi-layer $MoSe_2$ flakes.

A more detailed knowledge of the number of layers constituting the sample under investigation from Raman scattering experiments can be grasped from the observation of the A'$_1$/A$_{1g}$ feature close to 242 cm^{-1} (see Fig. 3c). Indeed, as already reported[22], this peak has an energy that depends on the number of layers, appears in the Raman scattering spectrum as a single component feature for 1L-$MoSe_2$ and 2L-$MoSe_2$, splits into two components for 3L-$MoSe_2$ and 4L-$MoSe_2$ and into three components for 5L-$MoSe_2$ and 6L-$MoSe_2$. The splitting, which comes from interlayer interactions in multilayer materials ($N > 2$)[20,29,43], can be used to determine the number of layers. Close to 252 cm^{-1}, another Raman scattering feature is observed with an energy that changes with the number of layer. Even though the proper origin of this feature is still unknown, its energy difference with the A'$_1$/A$_{1g}$ feature can provide an additional check for the number of layers of $MoSe_2$ (see appendix). In NL-$MoSe_2$, the contribution of acoustical phonons is also observed in the Raman scattering spectrum in the form of a rich series of overtones, as already discussed in the case of the monolayer.

To complete the description of the differences between mono- and multilayers, we note that another striking difference is seen at low vibrational frequencies, below 50 cm^{-1}. In multilayers, as can be observed in Fig. 3a, some additional features appear in that range with an energy that strongly depends on the number of layers. These modes are the shear and breathing modes of the multilayer structure, i.e. rigid vibrations of the whole layers with respect to each other. The evolution of these modes with increasing number of layers has recently been discussed in the case of $MoSe_2$[44]. One can notice from the spectra presented in Fig. 3a that, when measured with a 476 nm excitation, the intensity of these modes is comparable with that of the E"/E$_{1g}$ and A"$_2$/A$_{1g}$ modes discussed previously.

When changing the excitation laser energy, all the Raman scattering features considered so far show particular resonances. These resonances for one- to four- layer flakes, are presented in Fig. 4 for the E"/E$_{1g}$ phonon at 170 cm^{-1} (panel a), the A'$_1$/A$_{1g}$ phonon close to 242 cm^{-1} (panel b), the E'/E$_g$ phonon close to 290 cm^{-1} (panel c), for the A"$_2$/A$_{1g}$ phonon at 354 cm^{-1} (panel d), and for the 3LA(M) replica (panel d). The E"/E$_{1g}$ and A"$_2$/A$_{1g}$ Raman modes at 170 cm^{-1} and at 354 cm^{-1}, respectively, typical for multilayers, are only observed for excitation energies above 2.2 eV. They both exhibit a resonance close to 2.5 eV. For mono- and multilayers, we observe a resonance of the LO E'/E$_g$ phonon ($\sim$ 292 cm^{-1}) with the A and B excitons at 1.6 and 1.8 eV, respectively, while the TO E'/E$_g$ phonon ($\sim$ 289 cm^{-1}) has an intensity that increases when exciting at higher energy,close to the C excitons at 2.4 eV. As a results, in our experiments, these two LO and TO phonons cannot be observed simultaneously. On top of these resonances, the intensity of the TO E'/E$_g$ mode appears to continuously increase when increasing the excitation laser energy. In the case of the monolayer, for which these two features are the most pronounced, the resonance appears at a slightly higher excitation energy, close to 2.6 eV.

The main A'$_1$/A$_{1g}$ feature close to 242 cm^{-1} (Fig. 4b) is observed for all samples and shows for the 1L-$MoSe_2$ a resonance at high energy close to 2.6 eV, which corresponds to the C-exciton energy[26]. For higher number of layers, this high energy resonance appears at an energy close to 2.4 eV. A second resonance is observed at 1.8 eV

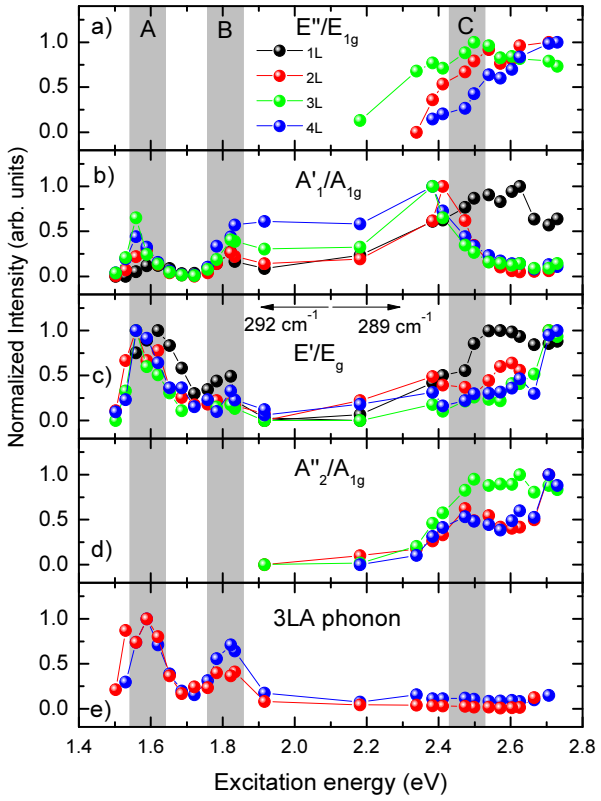

Figure 4. Normalized intensity of a) the E"/E_{1g} mode at 170 cm^{-1}, b) the A'$_1$/A_{1g} mode at 242 cm^{-1}, c) the E'/E_g modes around 290 cm^{-1}, d) the A"/A_{1g} modes at 354 cm^{-1}, and the 3LA phonon replica at 455 cm^{-1}, as a function of the excitation laser energy for 1L-$MoSe_2$ (black dots), 2L-$MoSe_2$ (red dots), 3L-$MoSe_2$ (green dots) and 4L-$MoSe_2$ (blue dots). The shaded regions represents the range of energy for the A, B and C excitons.

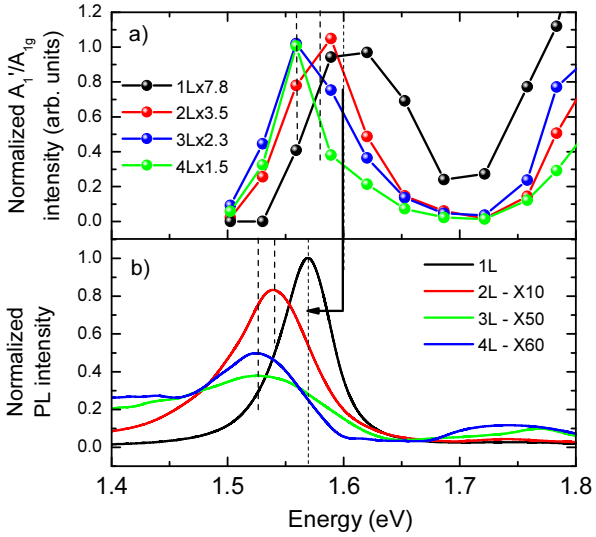

Figure 5. a) Normalized intensity of the A_1 mode at 242 cm^{-1} as a function of the excitation laser energy. b) Photoluminescence intensity, normalized to the maximum intensity of the monolayer. Vertical dashed lines indicate the observed maxima of Raman intensities (panel a) and of luminescence (panel b). Note the shift between the two maxima (highlighted with the vertical arrow, and equal to the energy of the involved phonon), indicative of an outgoing resonance process.

and corresponds to the B exciton. Within the resolution of our experiment, the energy of the resonance does not seem to depend on the number of layers. Lowering further the excitation laser energy, another resonance is observed. As for the LO E'/E_g feature, this resonance occurs close to 1.6 eV and its energy strongly changes with the number of layers. The energies of the A- and of the C- exciton energies appear to depend on the number of layers while the energy of the B excitons does not. Such evolution for the A, B and C excitons as a function of the number of layers has recently been observed in WSe_2 and in $MoSe_2$[45,46]. These results, concerning the various resonances observed for all the phonon modes of $MoSe_2$, appear as different as compared to the ones reported for MoS_2, where the A-type phonon mode shows a resonance with the high-energy exciton only while the E-type modes show a resonance with exclusively the low-energy A and B excitons[17]. In $MoSe_2$, the A'$_1$/A_{1g} mode shows clear resonances with all three types of excitons, while the E'/E_g LO phonon displays a resonance with the A and B excitons and the E'/E_g TO phonon only appears at high excitation energy.

Some modes, namely the E'/E_g and the A"$_2$/A_{1g}, have an intensity that, on top of the resonances observed at the exciton energies, increases strongly when increasing the excitation laser energy. This second resonance could be related to the valence band, and especially the band located $\sim$ 2 eV below the highest valence band at the K point[13,24,47]. In this range of energy, the partial density of states shows a maximum that could explain the resonance behavior observed in Raman scattering. This hypothesis needs to be further clarified on a theoretical point of view and/or with Raman scattering experiments performed in the UV range of energy. Finally, in contrast to the case of optical phonon modes described above, the LA phonon replicas show a pronounced resonance only with the low energy A and B modes, and are only weakly visible when exciting at higher energy. This behavior is shown in Fig. 4e for the 2L and 4L-$MoSe_2$. Similar to the case of MoS_2[15], when using an excitation energy close to that of A or B excitons, these acoustical phonon replica can become the dominant contribution to Raman scattering spectrum of $MoSe_2$ (see spectrum at 676 nm in Fig. 1 and appendix).

The low-energy resonance of the A'$_1$/A_{1g} mode is presented in more detail in Fig. 5a for excitation energies between 1.4 and 1.8 eV. The photoluminescence (PL) of $MoSe_2$ mono-layers arises from the low-energy A exciton[48]. In Fig. 5b, the room-temperature PL spectra recorded on the same samples are plotted for comparison with the data displayed in Fig. 5a.

When increasing the number of layers, we observe at

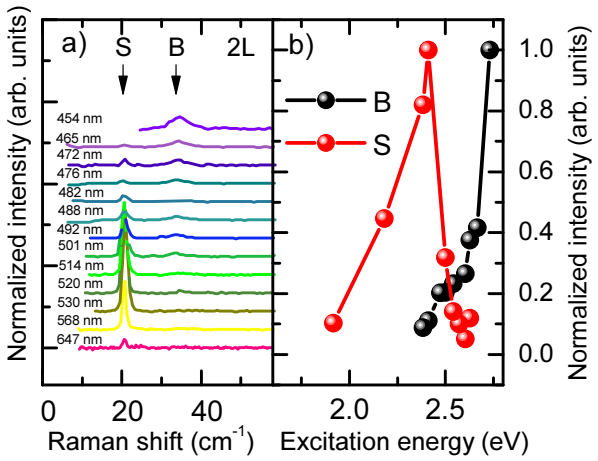

Figure 6. a) Raman scattering spectra of 2L-$MoSe_2$ for excitations energy ranging from 458 nm to 647 nm showing the shear (S) and breathing (B) modes. b) Evolution of the normalized intensity of the shear mode (red dots) and of the breathing mode (black dots) as a function of the excitation laser energy.

room temperature a marked decrease of the luminescence intensity together with a small shift of the luminescence energy, from 1.57 eV for 1L-$MoSe_2$, to 1.54 eV for 2L-$MoSe_2$, and to 1.52 eV for 3L- and 4L-$MoSe_2$. The origin of these two effects is still debated. They could originate (i) from a direct to indirect band gap transition when going from mono to multilayers, or (ii) reflect the difference in the relative energies of the A exciton and of the single particle indirect bandgap due to the change of dielectric screening and the decrease of the exciton binding energy for multilayers. The observed resonances for the A'$_1$/A_{1g} Raman scattering feature are centered at 1.610 ± 0.01, 1.575 ± 0.003, 1.560 ± 0.002 and 1.560 ± 0.002 eV for 1L- to 4L-$MoSe_2$, respectively. We interpret the energy difference between the emission of A excitons and the resonance in the Raman scattering as a signature of an efficient outgoing resonance. In fact, the maximum intensity of the Raman scattering is observed in this material when the incoming photon energy is equal to the sum of the exciton and of the scattered phonon energies.

As already mentioned, layered materials also show low-energy shear phonon modes, of the E-type symmetry, and breathing phonon modes, of the A-type symmetry. Detailed investigation of these modes in few-layer samples has recently become more accessible due to the commercial development of volume Bragg grating filters allowing to easily explore the low-energy range[49] of the Raman scattering spectrum, down to 5-10 cm^{-1}. The shear and breathing modes are today the subject of intense research in the field of MX_2. Their Raman shift as a function of the number of layers and their polarization selection rules have been described in detail for MoS_2, WSe_2, $MoSe_2$, WS_2 and in $MoTe_2$[29,34,35,44]. Because of technical difficulties, such studies are usually performed at a single excitation wavelength, and a complete picture of the excitation profile of such low energy modes in MX_2 is still lacking. Resonant Raman spectroscopy of such low-energy modes has been performed in semi-metallic twisted graphene, allowing to trace the evolution of its high-energy bands and to quantify the interlayer interaction as a function of the twist angle[50].

The use of a triple spectrometer and the access to large number of laser lines has allowed us to perform such a detailed resonant study for mono and multilayer $MoSe_2$. In Fig. 6a, we present Raman scattering spectra of the shear (S) and breathing (B) modes of 2L-$MoSe_2$ measured for excitation wavelengths from 454 nm to 647 nm. They are observed at 21 cm^{-1} and 34 cm^{-1}, respectively[44] and their energies do not change with the excitation wavelength. Fig. 6b illustrates the evolution of the normalized intensity of these two modes as a function of the excitation laser energy. As can be seen, they show rather distinct resonance behaviors. The E-type symmetry shear mode exhibits a pronounced resonance close to $\sim$ 2.4 eV, similar to the resonance observed for both high-energy A-type modes, which corresponds to the C exciton energy in 2L-$MoSe_2$. In contrast, the breathing mode, of the A-type symmetry, does not show this resonance but its intensity increases with increasing excitation laser energy. At excitation energies below 2.4 eV, the intensity of the breathing mode is nearly not observable in 2L-$MoSe_2$, grows rapidly at higher energies, becoming stronger than that of the shear mode and eventually representing the most pronounced low energy feature above 2.65 eV. For excitation energies lower than 1.95 eV (647 nm), we could not observe these low-energy modes mainly because of the strong low-energy scattering and/or PL when approaching the energies of the A and B excitons. Similar to the TO E'/E_g at 289 cm^{-1} and to the A"$_2$/A_{1g} mode at 354 cm^{-1}, the breathing mode's intensity seems to show a resonance with electronic excitations above the energy of the C exciton. For different MX_2 materials, depending on the excitation laser and on the exciton energy structure, very different intensity ratios between the shear and breath modes have been reported recently[19,29,34,35,44]. As follows from the study reported here, these differences arise from the peculiar resonance effect affecting differently the two modes.

To conclude, we have presented a comprehensive Raman scattering study of $MoSe_2$ mono- and multi-layers. We have shown in this compound the existence of new Raman modes which are only active in multilayers, and described their resonances when tuning the excitation laser energy across the three different excitons of this material. Resonant Raman spectroscopy appears as a well adapted tool to study a variety of excitons in thin layers of MX_2 and their coupling to optical phonons. Our experiments confirm the lowering of the A exciton's energy when increasing the number of layers and this result is corroborated by the PL measurements. We also show symmetry-dependent exciton-phonon coupling, in particular, we show experimentally that the low-energy shear mode of a bilayer displays a a pronounced resonance with

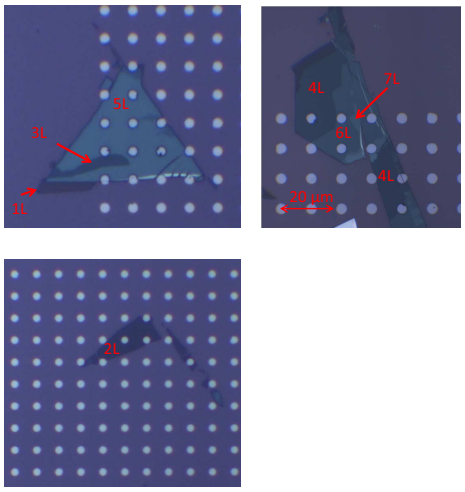

Figure 7. Three optical photographs of the same wafer with different locations corresponding to 1L, 2L, 3 L, 4 L, 5L and 6 L $MoSe_2$ specimens.

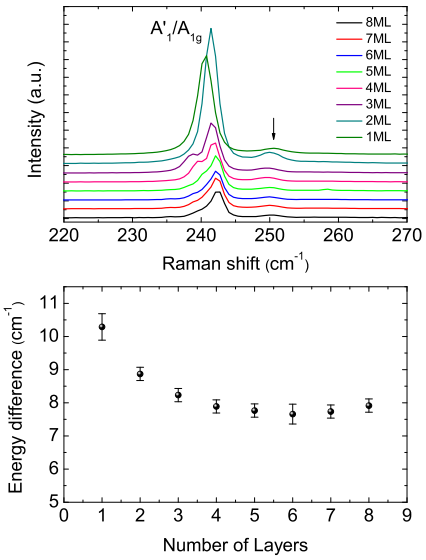

Figure 8. Upper panel: Raman scattering spectra for 1L to 8L-$MoSe_2$ samples. Lower panel: Energy difference between the 252 cm^{-1} feature and the A'$_1$/A_{1g} feature. The energy separation between these modes is maximum in the case of the monolayer and then decreases for thicker samples. The arrow in the top panel indicates the Raman scattering feature observed close to 250 cm^{-1}.

the C exciton while the breathing mode does not. On the other hand, this latter mode, together with the E'/E_g and A"$_2$/A_{1g} mode have an intensity that grows with the excitation laser energy, which is a signature of a still unexplored resonance at higher energy, in the deep UV range.

ACKNOWLEDGMENTS

We acknowledge fruitful discussions with S. Berciaud, M. Molas and with M. Potemski. Part of this work has been supported by the TWINFUSYON project, the graphene flagship project and by the European Research Council (ERC-2012-AdG-320590-MOMB).

I. APPENDIX

A. Photograph of the different $MoSe_2$ specimens

Large flakes of $MoSe_2$ mono- and multi-layers have been produced by mechanical exfoliation of bulk $MoSe_2$. Flakes were then deposited on a Si/SiO_2 substrate with 90 nm of SiO_2. The substrate had been patterned with circular holes of 6 μm diameter, but all the results presented in the main text have been obtained on supported regions. The following photograph in Fig. 7 present the different specimens that were used for the reported measurements.

B. Raman scattering features at 242 and 252 cm^{-1}

As stated in the main text, $MoSe_2$ mono-layers can be identified by (i) a single component A'$_1$ feature at 240 cm^{-1} while this feature is observed at 242.5 cm^{-1} for 2L and is a multi-component feature for $N > 2$, (ii) the non-observation of the two E"/E_{1g} and A"$_2$/A_{1g} modes at 170 and 354 cm^{-1}, respectively, and (iii) by the observation of an energy separation bigger than 9 cm^{-1} between the A'$_1$ and the feature close to 252 cm^{-1} (see Fig. 8. These ar the three Raman scattering signatures of 1L-$MoSe_2$ that emerge from this study.

C. Spectra normalization procedure

The normalization of Raman scattering intensities is crucial for the study of resonance effects. All intensities presented in the main text are normalized according to the following procedure: We first make a background correction. This background is most of the case flat but, when the excitation wavelength is set close to the low energy excitons of mono or few layer $MoSe_2$, luminescence signals affect the spectra and are removed but using standard computer tools. Spectra are then normalized by the integrated silicon signal at 522 cm^{-1}. The silicon first order Raman scattering peak shows a resonance when using high excitation energies. This effect was studied in detail in Ref. [32] and has to be taken into account by normalizing the measured signal by the resonance curve of silicon (which also includes the wavelength dependance of the Raman scattering process). Finally, the flake is

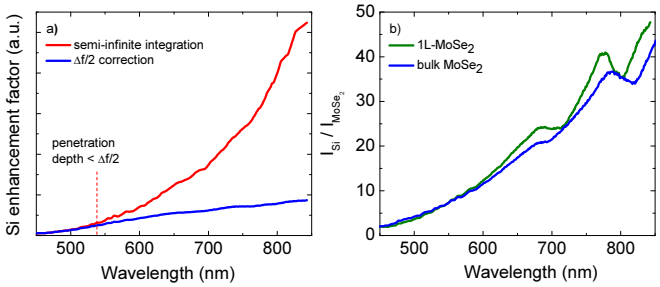

Figure 9. a) Interference enhancement factor for the Si Raman signal (I_{Si}) as a function of wavelength for a semi-infinite integration and the $\Delta f/2$ correction. When the penetration depth is smaller than $\Delta f/2$, (400 - 550 nm) the I_{Si} factor is approximately the same for both calculations. b) Ratio I_{Si}/I_{MoSe_2} for 1L-$MoSe_2$ and for bulk $MoSe_2$.

on top of a SiO_2/Si structure which produces optical interferences which have a strong impact on the measured Raman intensities. As it is shown in the literature[17,33,51], the Raman intensities of the Si and the $MoSe_2$ layers are proportional to an *enhancement factor* due to the optical interference existent in a multi-layered structure given by:

$$I_{MoSe_2} = \int_0^d |E_{ex}(x)E_{sc}(x)|^2 dx, \tag{1}$$

where $E_{ex}(x)$ and $E_{sc}(x)$ are the electrical field's amplitude of the total incident and scattered light respectively, and d is the thickness of the $MoSe_2$. The enhancement factor for the Si substrate is[17,33]

$$I_{Si} = \int_0^\infty |F_{ex}(x)F_{sc}(x)|^2 dx, \tag{2}$$

where $F_{ex}(x)$ and $F_{sc}(x)$ are the electrical field amplitude of the total incident and scattered light respectively. It is important to take into account the wavelength dependence of the complex refractive index of each materials to describe the propagation of the incident and of the scattered light. In the experiment, the incident wavelength is given by the exciting laser and the Raman process defines the scattered wavelength. To correct the data, we multiply the experimental spectra by the ratio I_{Si}/I_{MoSe_2}[17,33] after performing the silicon signal normalization described above.

Expression (2) is calculated considering an "unidimensional" problem, where the Si substrate is treated as a half-infinite media. In the IR region, where the Si absorption is small, when using a microscope objective with a large numerical aperture, we should take the divergence effect of the focused gaussian beam into account and calculate the integral in a probed volume defined by the depth of focus. The depth of focus Δf is defined as the distance between the points at each side of the beam-waist where the irradiance of the beam falls to one-half of its value[52]. According to Ref. [52] it is given by

$$\Delta f = \frac{\pi(2w_0)^2}{2\lambda}, \tag{3}$$

where w_0 is the beam radius at the waist (spot size in the focus) and λ is the wavelength within the material. Taking that into account, the upper integral limit(∞) must be modified to $\Delta f/2$.

For 1L-$MoSe_2$ sample, Fig. 9a shows the comparison between the semi-infinite integration and the $\Delta f/2$ correction for the Si Raman intensity both as a function of wavelength. Here we assumed a Raman shift of 520 cm^{-1}. The complex refractive index for Si and SiO_2 as a function of the wavelength were taken from Ref. [53] and Ref. [54] respectively and the refractive index of 1L-$MoSe_2$ was taken from Ref. [26]. Fig. 9b shows the ratio of the Si and the $MoSe_2$ enhancement factor as a function of the wavelength for a 1L-$MoSe_2$ and bulk $MoSe_2$ assuming a Raman shift of 290 cm^{-1}. The bulk $MoSe_2$ refractive index was taken from Ref. [33]. As can be seen, the enhancement factor for 1L-$MoSe_2$ and bulk $MoSe_2$ are similar so that we used the refractive index of the 1L-$MoSe_2$ for the calculations in the multi-layer samples.

* clement.faugeras@lncmi.cnrs.fr

[1] K. F. Mak, C. Lee, J. Hone, J. Shan, and T. F. Heinz, Phys. Rev. Lett. **105**, 136805 (2010).
[2] Q. Wang, K. Kalantar-Zadeh, A. Kis, J. Coleman, and M. Strano, Nat. Nanotech. **7**, 699 (2012).
[3] D. Xiao, G.-B. Liu, W. Feng, X. Xu, and W. Yao, Phys. Rev. Lett. **108**, 196802 (2012).
[4] X. Xu, W. Yao, D. Xiao, and T. F. Heinz, Nat. Phys. **10**, 343 (2014).
[5] B. Radisavljevic, A. Radenovic, J. Brivio, V. Giacometti, and A. Kis, Nat. Nanotech. **6**, 147 (2011).
[6] Z. Yin, H. Li, H. Li, L. Jiang, Y. Shi, Y. Sun, G. Lu, Q. Zhang, X. Chen, and H. Zhang, ACS Nano **6**, 74 (2012).
[7] T. Georgiou, R. Jalil, B. D. Belle, L. Britnell, R. V. Gorbachev, S. V. Morozov, Y.-J. Kim, A. Gholinia, S. J. Haigh, O. Makarovsky, L. Eaves, L. A. Ponomarenko, A. K. Geim, K. S. Novoselov, and A. Mishchenko, Nat. Nano. **8**, 100 (2013).
[8] A. K. Geim and I. V. Grigorieva, Nature **499**, 419 (2013).
[9] F. Withers, O. Del Pozo-Zamudio, A. Mishchenko, A. P. Rooney, A. Gholinia, K. Watanabe, T. Taniguchi, S. J. Haigh, A. K. Geim, A. I. Tartakovskii, and K. S. Novoselov, Nat. Mat. **14**, 301 (2015).
[10] K. He, N. Kumar, L. Zhao, Z. Wang, K. F. Mak, H. Zhao, and J. Shan, Phys. Rev. Lett. **113**, 026803 (2014).

[11] A. Chernikov, T. C. Berkelbach, H. M. Hill, A. Rigosi, Y. Li, O. B. Aslan, D. R. Reichman, M. S. Hybertsen, and T. F. Heinz, Phys. Rev. Lett. **113**, 076802 (2014).

[12] G. Scholes and G. Rumbles, Nat. Mat. **5**, 683 (2006).

[13] M. M. Ugeda, A. J. Bradley, S.-F. Shi, F. H. da Jornada, Y. Zhang, D. Y. Qiu, W. Ruan, S.-K. Mo, Z. Hussain, Z.-X. Shen, F. Wang, S. G. Louie, and M. F. Crommie, Nat. Mat. **13**, 1091 (2014).

[14] C. Lee, H. Yan, L. E. Brus, T. F. Heinz, J. Hone, and S. Ryu, ACS Nano **4**, 2695 (2010).

[15] K. Golasa, M. Grzeszczyk, P. Leszczynski, C. Faugeras, A. A. L. Nicolet, A. Wysmolek, M. Potemski, and A. Babinski, Appl. Phys. Lett. **104** (2014), 10.1063/1.4867502.

[16] E. del Corro, H. Terrones, A. Elias, C. Fantini, S. Feng, M. A. Nguyen, T. E. Mallouk, M. Terrones, and M. A. Pimenta, ACS Nano **8**, 9629 (2014).

[17] B. R. Carvalho, L. M. Malard, J. M. Alves, C. Fantini, and M. A. Pimenta, Phys. Rev. Lett. **114**, 136403 (2015).

[18] N. Scheuschner, R. Gillen, M. Staiger, and J. Maultzsch, Phys. Rev. B **91**, 235409 (2015).

[19] J.-U. Lee, J. Park, Y.-W. Son, and H. Cheong, Nanoscale **7**, 3229 (2015).

[20] T. Sekine, M. Izumi, T. Nakashizu, K. Uchinokura, and E. Matsuura, Jour. of the Phys. Soc. of Japan **49**, 1069 (1980).

[21] S. Tongay, J. Zhou, C. Ataca, K. Lo, T. S. Matthews, J. Li, J. C. Grossman, and J. Wu, Nano Letters **12**, 5576 (2012).

[22] P. Tonndorf, R. Schmidt, P. Böttger, X. Zhang, J. Börner, A. Liebig, M. Albrecht, C. Kloc, O. Gordan, D. R. T. Zahn, S. M. de Vasconcellos, and R. Bratschitsch, Opt. Express **21**, 4908 (2013).

[23] N. Kumar, Q. Cui, F. Ceballos, D. He, Y. Wang, and H. Zhao, Nanoscale **6**, 4915 (2014).

[24] S. Horzum, H. Sahin, S. Cahangirov, P. Cudazzo, A. Rubio, T. Serin, and F. M. Peeters, Phys. Rev. B **87**, 125415 (2013).

[25] A. Molina-Sánchez and L. Wirtz, Phys. Rev. B **84**, 155413 (2011).

[26] Y. Li, A. Chernikov, X. Zhang, A. Rigosi, H. M. Hill, A. M. van der Zande, D. A. Chenet, E.-M. Shih, J. Hone, and T. F. Heinz, Phys. Rev. B **90**, 205422 (2014).

[27] M. Yamamoto, S. T. Wang, M. Ni, Y.-F. Lin, S.-L. Li, S. Aikawa, W.-B. Jian, K. Ueno, K. Wakabayashi, and K. Tsukagoshi, ACS Nano **8**, 3895 (2014).

[28] C. Ruppert, O. B. Aslan, and T. F. Heinz, Nano Letters **14**, 6231 (2014).

[29] G. Froehlicher, E. Lorchat, F. Fernique, C. Joshi, A. Molina-Sanchez, L. Wirtz, and S. Berciaud, Nano Letters **0**, null (0).

[30] X. Luo, Y. Zhao, J. Zhang, M. Toh, C. Kloc, Q. Xiong, and S. Y. Quek, Phys. Rev. B **88**, 195313 (2013).

[31] H. Terrones, E. Del Corro, S. Feng, J. M. Poumirol, D. Rhodes, D. Smirnov, N. R. Pradhan, Z. Lin, M. A. T. Nguyen, A. L. Elias, T. E. Mallouk, L. Balicas, M. A. Pimenta, and M. Terrones, Scientific Reports **4** (2014), 10.1038/srep04215.

[32] J. B. Renucci, R. N. Tyte, and M. Cardona, Phys. Rev. B **11**, 3885 (1975).

[33] S.-L. Li, H. Miyazaki, H. Song, H. Kuramochi, S. Nakaharai, and K. Tsukagoshi, ACS Nano **6**, 7381 (2012).

[34] X. Zhang, W. P. Han, J. B. Wu, S. Milana, Y. Lu, Q. Q. Li, A. C. Ferrari, and P. H. Tan, Phys. Rev. B **87**, 115413 (2013).

[35] Y. Zhao, X. Luo, H. Li, J. Zhang, P. T. Araujo, C. K. Gan, J. Wu, H. Zhang, S. Y. Quek, M. S. Dresselhaus, and Q. Xiong, Nano Lett. **13**, 1007 (2013).

[36] D. J. Late, S. N. Shirodkar, U. V. Waghmare, V. P. Dravid, and C. N. R. Rao, ChemPhysChem **15**, 1592 (2014).

[37] A. Berkdemir, H. R. Gutierrez, A. R. Botello-Mendez, N. Perea-Lopez, A. L. Elias, C.-I. Chia, B. Wang, V. H. Crespi, F. Lopez-Urias, J.-C. Charlier, H. Terrones, and M. Terrones, Scientific Rep. **3** (2013), 10.1038/srep01755.

[38] B. Chakraborty, H. Matte, A. Sood, and C. Rao, J. Raman Spectrosc. **44**, 92 (2013).

[39] K. Golasa, M. Grzeszczyk, R. Bozek, P. Leszczynski, A. Wysmolek, M. Potemski, and A. Babinski, Solid State Comm. **197** (2014), 10.1016/J.ssc.2014.08.009.

[40] J.-U. Lee, K. Kim, and H. Cheong, 2D Materials **2**, 044003 (2015).

[41] D. Y. Qiu, F. H. da Jornada, and S. G. Louie, Phys. Rev. Lett. **111**, 216805 (2013).

[42] A. J. Bradley, M. M. Ugeda, F. H. da Jornada, D. Y. Qiu, W. Ruan, Y. Zhang, S. Wickenburg, A. Riss, J. Lu, S.-K. Mo, Z. Hussain, Z.-X. Shen, S. G. Louie, and M. F. Crommie, Nano Lett. **15**, 2594 (2015).

[43] J. L. Verble and T. J. Wieting, Phys. Rev. Lett. **25**, 362 (1970).

[44] S.-Y. Chen, C. Zheng, M. S. Fuhrer, and J. Yan, Nano Lett. **15**, 2526 (2015).

[45] A. Arora, M. Koperski, K. Nogajewski, J. Marcus, C. Faugeras, and M. Potemski, Nanoscale **7**, 10421 (2015).

[46] A. Arora, K. Nogajewski, M. Molas, M. Koperski, and M. Potemski, Nanoscale **7**, 20769 (2015).

[47] G. Wang, C. Robert, A. Suslu, B. Chen, S. Yang, S. Alamdari, I. C. Gerber, T. Amand, X. Marie, S. Tongay, and B. Urbaszek, ArXiv e-prints (2015), arXiv:1506.08114 [cond-mat.mtrl-sci].

[48] D. MacNeill, C. Heikes, K. F. Mak, Z. Anderson, A. Kormányos, V. Zólyomi, J. Park, and D. C. Ralph, Phys. Rev. Lett. **114**, 037401 (2015).

[49] P. H. Tan, W. P. Han, W. J. Zhao, Z. H. Wu, K. Chang, H. Wang, Y. F. Wang, N. Bonini, N. Marzari, N. Pugno, G. Savini, A. Lombardo, and A. C. Ferrari, Nat. Mat. **11**, 294 (2012).

[50] J.-B. Wu, X. Zhang, M. Ijaes, W.-P. Han, X.-F. Qiao, X.-L. Li, D.-S. Jiang, A. C. Ferrari, and P.-H. Tan, Nat. Comm. **5** (2014), 10.1038/ncomms6309.

[51] D. Yoon, H. Moon, Y.-W. Son, J. S. Choi, B. H. Park, Y. H. Cha, Y. D. Kim, and H. Cheong, Phys. Rev. B **80**, 125422 (2009).

[52] J. A. M. B. M. Delhaye, J. Barbillat and E. D. Silva, *Raman Microscopy, development and applications* (Academic Press, 1996).

[53] E. Palik, *Handbook of Optical Constants of Solids*, Vol. 3 (Academic Press, 1998).

[54] I. H. Malitson, J. Opt. Soc. Am. **55**, 1205 (1965).